A Study of the Crystallization of ZrO$_2$ in the Sol–Gel System: ZrO$_2$–SiO$_2$

D. H. Aguilar, L. C. Torres-Gonzalez, and L. M. Torres-Martinez

Facultad de Ciencias Quimicas, Division de Estudios Superiores, Universidad Autonoma de Nuevo Leon, A.P. 1864, Monterrey, Nuevo Leon, Mexico

T. Lopez

Departamento de Quimica, Universidad Autonoma Metropolitana-Iztapalapa, A.P. 55-534, 09340 Mexico, DF, Mexico

and

P. Quintana[1]

CINVESTAV-IPN-Unidad Merida, Antigua Carretera a Progreso Km. 6, A.P. 73 Cordemex, 97310 Merida, Yucatan, Mexico

ZrO$_2$–SiO$_2$ sol–gel powders were produced using tetraethoxysilane (TEOS) and zirconium propoxide. After gellation, the ZrO$_2$ crystallization process was investigated using X-ray diffraction (XRD), thermal analysis (DTA/TGA), and scanning electron microscopy (SEM). Fresh gels were amorphous. Thermal treatments were carried out from 100 to 1400°C for a total annealing time of 182 h. Tetragonal zirconia, Z(t) was the first phase to crystallize, between 300 and 500°C. Crystallization temperature was lower for zirconia-rich compositions, increasing as silica content was raised. DTA analysis showed that Z(t) crystallization occurred in two stages. Complete tetragonal–monoclinic zirconia transformation occurred near 1000°C, and was clearly observed only in ZrO$_2$-rich compositions (>80%). Silica remains amorphous until 1200°C, when ZrSiO$_4$ formation took place. A metastable sol-gel phase diagram was proposed to show the crystallization process between 100 and 1400°C. © 2001 Academic Press

Key Words: zirconia; phase transformation; silica; sol–gel; XRD; DTA/TGA; SEM.

1. INTRODUCTION

In recent years, considerable research has been done on the synthesis of advanced ceramic materials using the sol–gel technique. This kind of synthesis is important, as it allows the manufacture of quality materials with high purity and homogeneity, as well as control of particle size (1–10).

Zirconium oxide has beneficial ceramic properties such as chemical resistance, thermal stability, high mechanical toughness, and high-temperature ionic conductivity. As a result, it has been used widely in technological applications as varied as glass–ceramics, composites, and oxygen gas sensors. Depending on factors such as preparation method, pH, temperature, and kinetic mechanism, synthetic zirconia shows three crystalline phases: monoclinic, tetragonal, and cubic (11–14).

Several methods have been developed to stabilize the tetragonal phase at low temperatures. These include the addition of doppants (Y$_2$O$_3$, CaO, MgO, CeO$_2$), or the use of soft-chemistry methods, from which nanocrystalline materials can be obtained (15–20). Formation of the metastable tetragonal phase has been attributed to a number of factors, such as crystallite size, surface and lattice defects, adsorbed species on the surface, and domain boundary stresses (21–23).

When zirconia is prepared using the sol–gel method, the tetragonal phase can be stabilized at low temperatures, depending on pH and the hydrolysis catalysts used in the synthesis (24). The OH groups retained in the bulk in this method favor stabilization of the tetragonal phase, whereas when positive ions are present (e.g., H$^+$, Li$^+$, Na$^+$) the monoclinic phase is produced at low temperatures.

ZrO$_2$–SiO$_2$ mixed oxides prepared using the sol–gel technique are promising catalysts, or catalyst supports, in petrochemical processes. For example, it has been shown to be useful in the *n*-hexane isomerization reaction to high octane, employing bifunctional zirconia–silica catalysts in products such as 2,2-dimethylbutane and 2,3-dimethylbutane (14). When sulfated, these materials developed

---

[1] To whom correspondence should be addressed.

strong acidity, comparable to that obtained when H_2SO_4 is used for homogeneous catalyzed acidic reactions.

A high zirconia dispersion occurs in the silica matrix when zirconia is coprecipitated with silica. The mixed oxides exhibit high surface area and are highly hydroxylated (24–27). Due to their refractoriness, these mixed oxides are difficult to produce by conventional melting techniques, and thus the sol–gel method has been widely used for preparation of these materials at low temperatures (28–35).

A number of studies address the ZrO_2–SiO_2 system synthesized with the sol–gel method; however, most focus only on a few compositions, treated at low temperatures and with short annealing times. Miranda *et al.* (28, 29), synthesized samples ranging from 10 to 55% mol ZrO_2 annealed during 5.5 h at 550, 850, and 1600°C. Nagarajan and Rao (21) utilized only three compositions (5, 25, and 50% mol zirconia), annealing them for 2 h in temperatures ranging from 400 to 1500°C. Andrianainarivelo *et al.* (30) studied the crystallization behavior in four compositions (1, 10, 17, and 50% mol ZrO_2) at temperatures between 600 and 1300°C with heating times ranging from 2 to 5 h. Other studies have focused only on a small range of low zirconia content compositions (31–33) or with zirconia in amorphous state (34).

The objective of this paper is to present a systematic analysis of the crystallization process of amorphous sol–gel samples and the thermal behavior of zirconia cogelled with silica, in the complete ZrO_2–SiO_2 system range, annealing the samples with long thermal treatments at temperatures between 100–1400°C.

2. EXPERIMENTAL PROCEDURE

Different ZrO_2–SiO_2 system compositions were prepared employing the sol–gel method, using alcoxides. The starting materials were silicon tetraethoxysilane, TEOS (Aldrich, 98% in ethanol), and zirconium propoxide (Aldrich, 70% in ethanol).

Pure zirconia was obtained from hydrolysis of 14.5 ml of zirconium propoxide with 39 ml of EtOH, placed in a flask, in an argon atmosphere to avoid precipitation (35). The mixture was kept at 50°C for 1 h, under constant agitation. Gellation was induced by adding 2.4 ml of distilled water, drop by drop.

The silica was synthesized via acid hydrolysis of TEOS, using nitric acid as the catalyst. A 1:4 ml TEOS:EtOH ratio was kept at 70°C for 1 h under moderate agitation, at the end of which 1.6 ml of water was added. To cause gellation, the mixture was maintained under these conditions for an additional 3 h.

The mixed oxides were produced using cogellation, a procedure with four stages: TEOS prehydrolysis, addition of zirconium propoxide, complete hydrolysis, and gellation.

TABLE 1
Molar Relationships Used in Each Stage of the Synthesis of Different Samples with Composition (x) ZrO_2 $(1-x)$ SiO_2

TEOS prehydrolysis	
mol Si^{4+}	$(1-x)$
mol EtOH/mol Si^{4+}	15.5
mol H_2O/mol Si^{4+}	2.8
mol HNO_3/mol Si^{4+}	5×10^{-4}
Addition of zirconium propoxide	
mol Zr^{4+}	x
mol EtOH/mol Zr^{+4}	27.5
mol HNO_3/mol Zr^{+4}	2
Complete hydrolysis and gelation	
mol H_2O/mol Zr^{4+}	5.2

Samples of each composition (1 g) were obtained by dissolving TEOS with ethanol in argon atmosphere. The prehydrolysis condition was developed adding a small amount of water, less than the stoichiometric ratio. The solution was then maintained at 70°C under strong agitation for 4 h. After the prehydrolysis was attained, a mixture of EtOH and HNO_3 followed by zirconium propoxide (drop by drop) were added. The mixture was kept at 70°C under strong agitation for 3 h. Gellation was achieved by adding the amount of water necessary to complete the stoichiometric ratio, under slow agitation. The specific compositions synthesized were 20, 40, 50, 60, 80, 90, 95, 98, and 99% molar ZrO_2. The stoichiometric ratios used for the synthesis are shown in Table 1, and the synthesis procedure is illustrated in Fig. 1.

The opaque gels produced in the above procedure were dried at 100°C and then milled in an agate mortar for later thermal treatment and material characterization. The powders were placed in platinum crucibles, and each sample was subjected to a successive thermal treatment, with temperatures ranging from 100 to 1400°C. For this treatment, the temperature was increased in 100°C increments with a heating time of 14 h per increment and a total annealing time for the entire temperature range of 182 h (7.5 days).

X-ray powder diffraction patterns were registered using a D-5000 Siemens diffractometer with a monochromatic Cu$K\alpha$ radiation ($\lambda = 1.5418$ Å) and Ni filter. Patterns were recorded for routine analysis with a step size of 0.05° per second, from 18 to 110° 2θ. Thermal analysis was carried out in air with a simultaneous DTA/TGA (Thermal Instruments, SDT 2960), using 20 mg of as-obtained powders. The temperature range used was from 50 to 1200°C at a heating rate of 10°C/min. Calcined alumina was used as a reference.

For morphological characterization, the treated powders were pressed into pellets and coated with graphite. Micrographs were taken of the pellets with a scanning electron microscope (Leica LEO 5440).
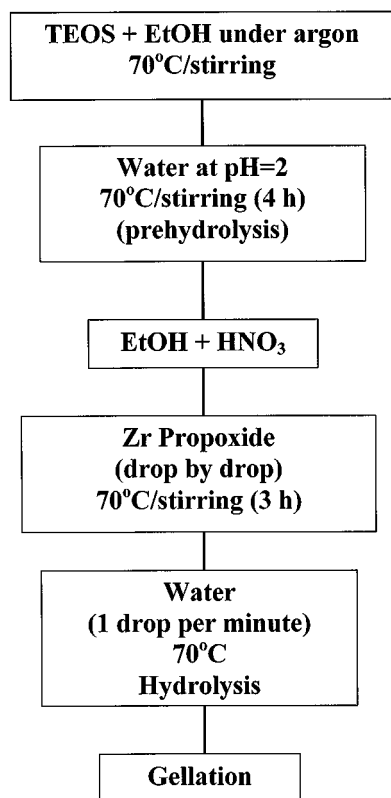
FIG. 1. Synthesis diagram for the mixed oxides.

3. RESULTS AND DISCUSSION

The crystallization process and thermal behavior of different compositions within the studied ZrO_2–SiO_2 system were analyzed both with XRD and DTA/TGA techniques. Figure 2 shows the X-ray diffractograms and the thermograms of some of the samples.

For pure zirconia gel annealed at 150°C (Fig. 2a), the XRD showed a pattern of nearly amorphous material. As temperature increased, broad peaks seen at lower temperatures became sharper, demonstrating the evolution of a crystalline phase, similar to the tetragonal form of zirconia, Z(t). With continued heating, Z(t) entered a continuous transformation into the monoclinic form, Z(m). At higher temperatures (900°C), the amount of Z(m) predominated and was completely pure after heating at 1100°C.

The DTA/TGA curve for the fresh samples (Fig. 2b) exhibited an endothermic peak at 97°C, due to desorption of water and ethanol occluded in the gel. Two exothermic peaks appeared at 318 and 393°C. These are related to loss of residual organic groups and dehydroxylation, as shown by the 12% weight loss recorded in the TGA, and a change in color. Another exothermal peak occurred at 443°C, which

is due to the partial transformation from the tetragonal to the monoclinic phase.

Crystallization of Z(t) in pure ZrO_2 prepared with sol–gel processes is reported to occur at low temperatures, around 300°C (24, 30, 35, 36). This is due to the formation of micro-crystalline zirconia and to preparation conditions (4, 37–39). When nanocrystalline nondoped zirconia is annealed, the tetragonal phase is transformed into the monoclinic phase (40, 41), a transformation that begins at approximately 450°C (24) and can be completed between 800 and 1000°C (19, 21, 30). In the present study, however, the formation of Z(t) was detected with XRD as beginning in the earliest stages of thermal treatment (150°C). The initial transformation to monoclinic phase occurred at 443°C. This was detected with DTA, but not observed with XRD, because the monoclinic phase has a smaller crystallite size than the tetragonal phase. The presence of Z(m) was confirmed at 500°C by recording the XRD pattern at a slower rate of 0.002°C per second.

Zirconia crystallization behavior was modified by addition of silicon oxide. For the $80ZrO_2$:$20SiO_2$ composition (Fig. 2c), XRD showed a nearly amorphous pattern, with traces of tetragonal zirconia microcrystals (600°C), indicated by an incipient peak at 30.2°(2θ). At higher temperature (700°C) a substantial increase in intensity was observed, though Z(t) remained pure until approximately 1100°C. Z(m) crystallized at 1200°C and reacted with amorphous silica to form $ZrSiO_4$ (ZS), with both phases coexisting at up to 1400°C. Worth mentioning is that at 1100°C, in the mixed oxides, Z(t) was still mainly in crystalline phase, whereas in pure zirconia it had already transformed to the monoclinic form.

The thermogram (Fig. 2d) shows an exothermic peak at 395°C, which is assigned to the formation of microcrystalline tetragonal zirconia (24), though this process was not observed in the XRD below 600°C. A second exothermic peak located at 755°C is ascribed to the bulk crystallization of Z(t), since the corresponding diffraction peaks clearly increase in the XRD (Fig. 2c).

When silica content increases similar results are obtained. In the composition $60ZrO_2$:$40SiO_2$ (Figs. 2e and 2f), tetragonal zirconia formed in two steps, initial and bulk crystallization, identified by the two DTA exothermic peaks at 398 and 855°C, respectively. The latter temperature agrees with the XRD patterns, where the Z(t) bulk crystallization peak is observed at 800°C.

At approximately 1200°C, polymorphic transformation of Z(t) to Z(m) occurred, and $ZrSiO_4$ formation (ZS) begins. As temperature increased, the relative intensity of the monoclinic zirconia peaks diminished considerably, whereas those corresponding to Z(t) did not change. ZS peaks also grew in intensity, suggesting that Z(m) reacts more easily with amorphous silica to form ZS, which was the main phase at 1400°C.

For the 40ZrO$_2$:60SiO$_2$ composition, the tetragonal phase was not observed until 900°C with XRD (Fig. 2g). This occurred because the amorphous silica concentration was higher than zirconia, making it difficult to detect the XRD peaks for Z(t) at lower temperatures. The addition of silica delayed Z(t) bulk crystallization, extending its higher stability limit to 1200°C, over 100°C more than in the previous composition. At 1300°C, ZS had already formed, and traces of monoclinic zirconia were observed. The

formation of ZS was complete at 1400°C, and the excess silica crystallized as cristobalite.

The DTA/TGA (Fig. 2h) showed an endothermic peak at 103°C, with a weight loss of 7.45% (in the range between 25 and 240°C), due to evaporation of water, solvent, and other residuals. A second weight loss of 9.17% occurred between 240 and 510°C, and is associated with sample dehydroxylation. The initial formation of Z(t) is indicated in the thermogram by a wide exothermic peak at approximately 400°C,
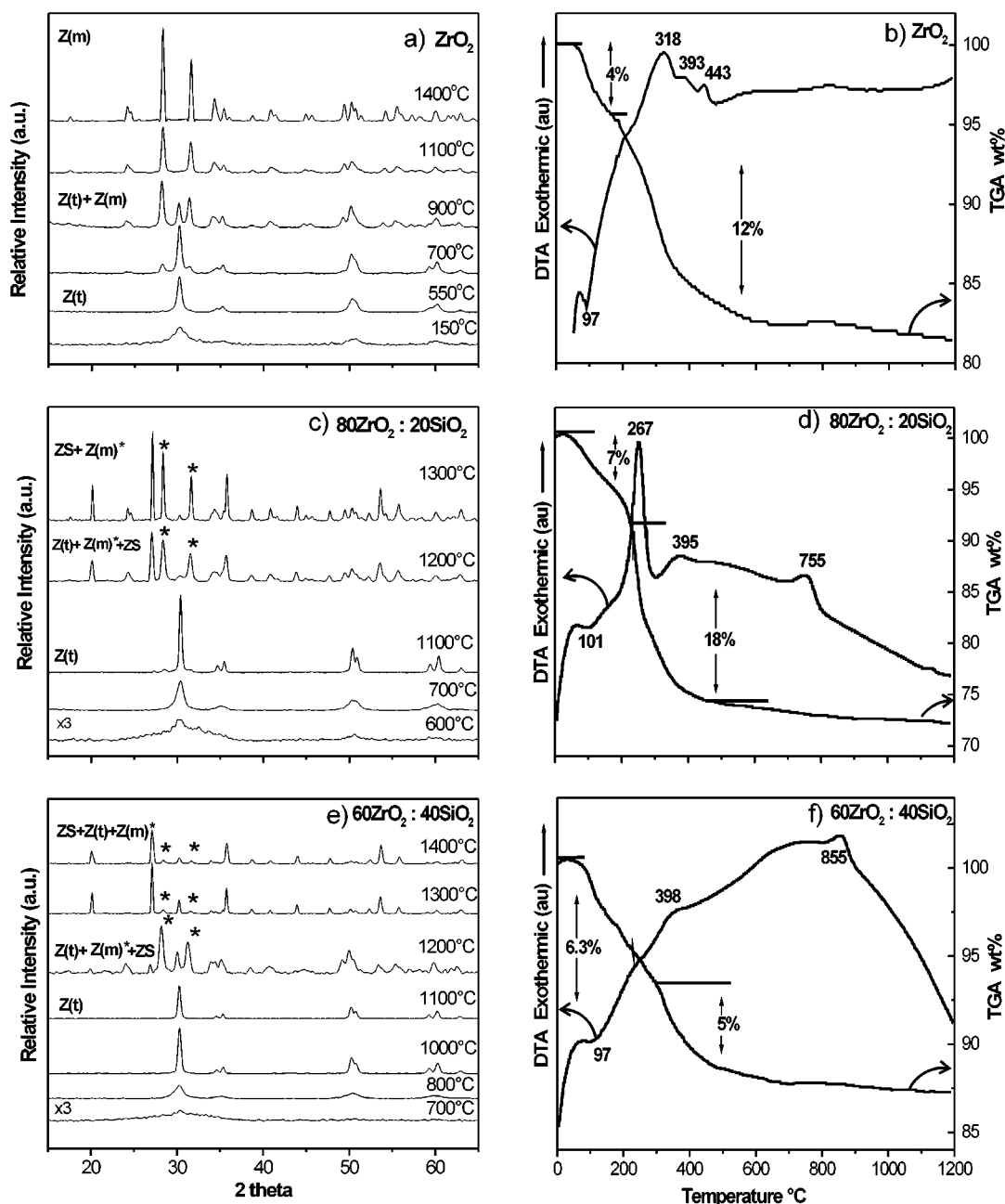

FIG. 2. Evolution of XRD and DTA/TGA with temperature for several compositions in the ZrO$_2$–SiO$_2$ system. Low peak intensity diffractograms were multiplied three times (×3) for better comparison.
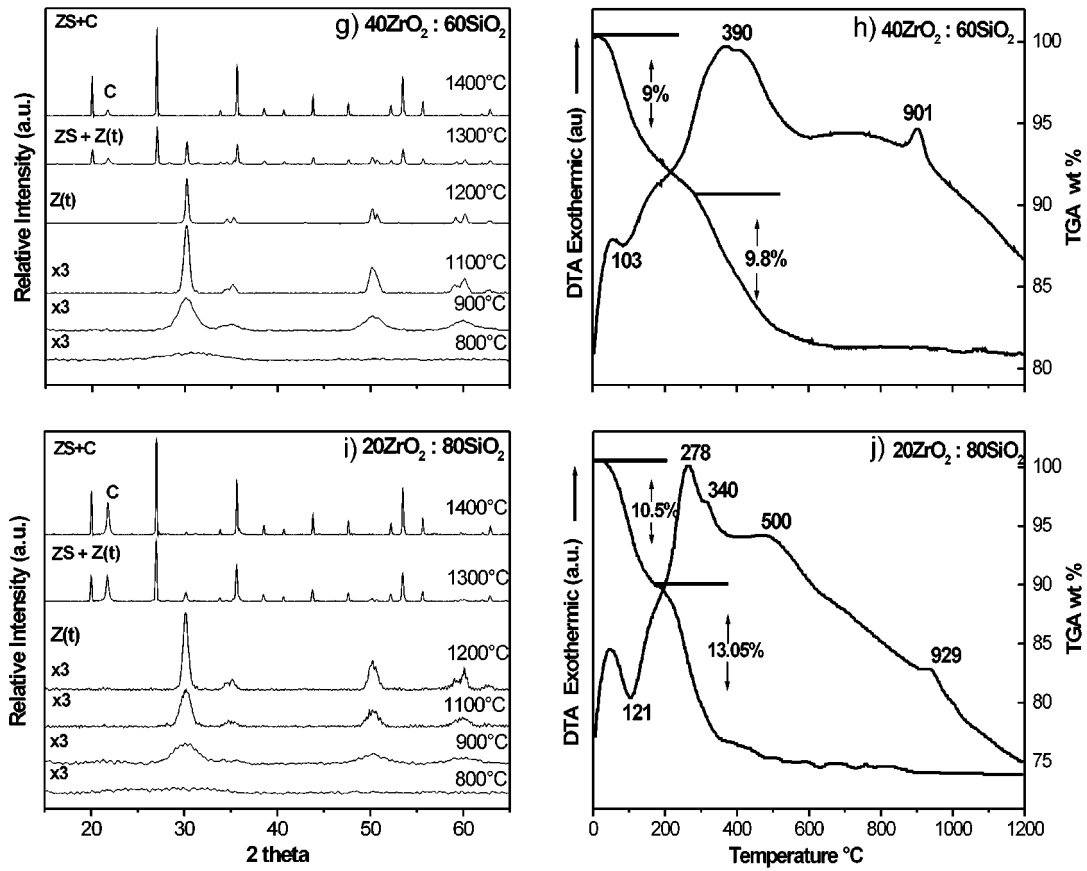
FIG. 2—Continued

and the second crystallization stage is denoted by another exothermic peak at 901°C.

The silica-rich composition 20ZrO$_2$:80SiO$_2$ (Figs. 2i and 2j) exhibited a strong endothermic peak at 121°C. This is 10–15°C higher than in the other compositions and is due to the high sol–gel silica concentration, which contains a high number of OH$^-$ groups (7). The presence of silanol groups generates the formation of hydrogen bridges and the existence of dipole–dipole interactions, requiring more energy to desorb the ethanol and water. In the interval up to 210°C, TGA (Fig. 2j) showed a weight loss of 10.5%, due to desortion of residual alcoxide, followed by a 13% loss between 210 and 390°C, which is ascribed to the high dehydroxylation of the mixed oxide.

Exothermic peaks were seen at 500°C for the initial Z(t) crystallization stage, and again at 929°C for the second Z(t) crystallization. At the higher temperature, the Z(t) diffraction peaks increased (Fig. 2i), becoming clearly developed. Tetragonal zirconia was found to coexist with amorphous silica up to 1200°C, though at higher temperatures only traces of Z(t) were detected, with ZS and cristobalite clearly observed.

Based on a combination of XRD and thermal analysis data, a phase diagram was constructed to show the

crystallization process in the ZrO$_2$–SiO$_2$ system (Fig. 3). Though this diagram does not represent a thermodynamic equilibrium phase diagram, it does show the temperature
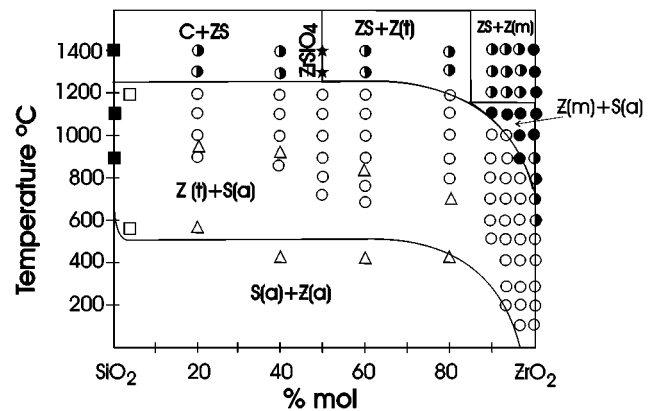

FIG. 3. Metastable phase diagram of the ZrO$_2$–SiO$_2$ system showing the phases formed at different annealing temperatures. Amorphous silica, S(a); amorphous zirconia, Z(a); tetragonal zirconia, Z(t); monoclinic zirconia, Z(m); zircon, ZS; cristobalite, C. XRD and DTA data for the crystallization of Z(t) are represented by ○ and △, respectively; □ data are obtained from references (21, 28, 30, 48); ★, ZS; ■, cristobalite; ●, Z (m); ◑, two crystalline phases.

and composition ranges of the different phases formed in the ZrO_2–SiO_2 system, synthesized by the sol–gel method. The studied temperature range is from 100 to 1400°C, with a total annealing time of 182 h.

The tetragonal phase was present from the as-made powders up to 500°C, in pure zirconia. Subsequently, the polymorphic transformation to the monoclinic phase begins (Fig. 3). Both phases continued to coexist up to 1000°C, though above this temperature only the monoclinic phase was observed.

In the entire system, the first phase to crystallize from the amorphous state was tetragonal zirconia. Comparing the X-ray diffraction pattern with the powder diffraction file (PDF-ICDD) data cards (42), a close similarity was seen between the tetragonal phase in the present study and that reported by Teufer (43). However, the positions of the peaks in the present study were shifted toward higher 2θ values. Therefore, the *a*- and *c*-lattice parameters calculated from the (012) and (210) peaks were 0.359 and 0.519 nm, respectively. These are similar to values obtained for zirconia doped with yttria (44, 45) or alumina (46).

Through DTA, the crystallization process of the metastable tetragonal phase was shown to occur in two steps. The initial Z(t) crystallization temperature was detected between 400 and 500°C, increasing as silica content rises. With further heating, a second crystallization stage occurred, shifting constantly toward higher temperature values as silica content increased. Both processes are indicated in the diagram with the symbol △. The earlier stages of Z(t) phase crystallization were difficult to detect with XRD, but later stages were clearly detectable due to a substantial increase in diffraction peak intensity (data denoted by ○).

Crystallization behavior for the 90, 95, and 98% mol ZrO_2 compositions was very similar (Fig. 4). In these mixtures, crystallization begins near 100°C, though the upper temperature limit is higher than for pure zirconia. This demonstrates that the addition of a small percentage of silica stabilizes the tetragonal phase. The tetragonal–monoclinic transformation occurred at 800°C for 99% mol ZrO_2, but was raised to above 1100°C for the 90% mol composition, with a small coexistence region between Z(m) and amorphous silica (denoted by ● in Fig. 3). At approximately 1200°C, both phases react to form zircon, the excess ZrO_2 remaining monoclinic.

In general, increases in silica content in the compositions used in the present study improves the thermal stability of Z(t), which is corroborated in other studies (16, 21). The upper stability limit of the tetragonal phase varied between 850 and 1200°C, depending on the ZrO_2/SiO_2 ratio. This means that the coexistence region between Z(t) and amorphous silica extends over a wide range of compositions and temperatures.
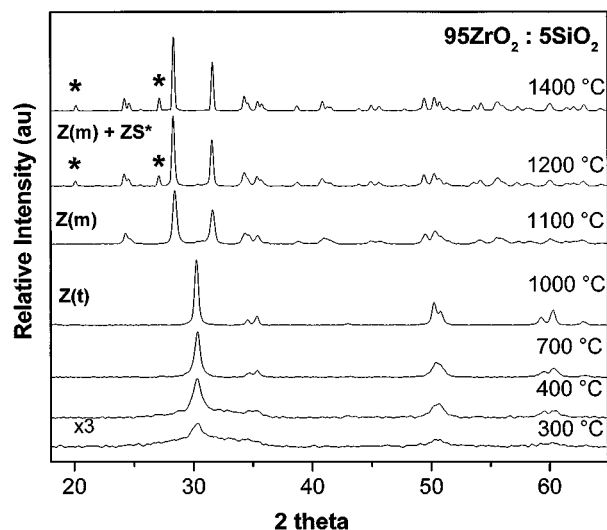

FIG. 4. X-ray diffractograms at different temperatures for $95ZrO_2:5SiO_2$ composition showing the presence of pure Z(t) up to 1000°C.

Zircon ($ZrSiO_4$) formation was studied in the stoichiometric composition, $50ZrO_2:50SiO_2$. In this composition, the tetragonal phase was detected, with XRD, from 800 to 1100°C. Crystallization of Z(m) occurred at approximately 1150°C, when it simultaneously began reacting with amorphous silica to form ZS (denoted by ★). Pure ZS was obtained when the mixture was heated at 1300°C for 50 h; according to the literature, the formation of zircon (without additives) requires higher temperatures (47). This formation is shown in Fig. 3, where zircon is a phase line separating regions of a mixture of two phases: on the left side of the diagram is ZS + cristobalite and on the right is ZS + Z(t).

Silica-rich compositions were not studied, though it is known (21, 28, 30, 48) that crystallization temperature increases up to 800°C (data denoted by □; Fig. 3). Pure silica, SiO_2, remained amorphous up to 900°C, then appears cristobalite (indicated by ■) (31), with crystallinity increasing with temperature up to 1400°C.

Tetragonal phase particle size during the crystallization process was determined with XRD (Scherrer method), by evaluating the FWHM of the (101) reflection peak using a profile fitting program (49). The crystallite size (Fig. 5) varied between 5 and 27 nm before the tetragonal–monoclinic transformation, depending on annealing temperature. This is lower than the theoretical critical size of 30 nm (18), but corresponds well with other experimental values (24). Notably, crystallite grain size growth in zirconia-rich compositions exhibited a plateau over a wide temperature range (from 450 to 800°C), but this plateau decreased and almost disappeared as the silica concentration increased (Fig. 5). Between 800 and 900°C the slope changed due to rapid grain growth in the fine grain matrix.
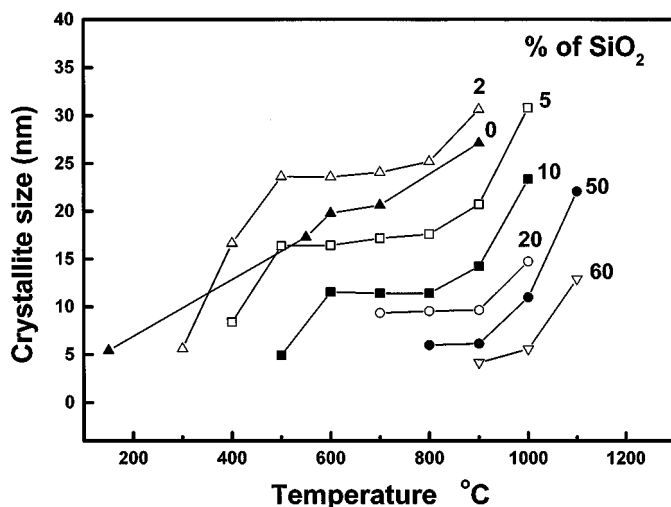
FIG. 5. Average crystallite size obtained from XRD measurements for tetragonal zirconia in several compositions at different annealing temperatures.

FIG. 6. SEM images showing morphology for pure ZrO$_2$. (a) Tetragonal phase at 550°C (500 ×, original magnification); (b) grain distribution of the m-ZrO$_2$ at 1250°C (2000 ×, original magnification).

In all cases, crystallite growth took place prior to the tetragonal–monoclinic transformation (23), though, by blocking grain growth, the low-expansivity silica matrix inhibited the monoclinic transformation and favored stability of the tetragonal phase in the mixed oxides. Thus, addition of silica helped maintain the zirconia particles below the critical size (16–18, 30).

In fact, the addition of silica greatly retarded the tetragonal–monoclinic transformation in zirconia, which did not occur until the samples were progressively heated to 1200°C during 168 h. This transformation in pure zirconia occurs after heating to 600°C for 84 h. This result contrasts with the results of other studies in which the transformation is reported to occur after only a few hours at high temperatures (16, 21, 28–30).

The morphology of the different compositions at various temperatures was analyzed with scanning electron microscopy. The images of pure ZrO$_2$ showed a distinct morphology. At 550°C, the tetragonal phase has a grain distribution with particles smaller than 5 μm and grains with flat surfaces and smooth edges (Fig. 6a). A drastic morphology change occurred at the tetragonal-monoclinic transformation, when the grains acquired a spherical shape with homogeneous grain distribution, and a particle size varying between 5 to 1 μm (Fig. 6b).

For the mixed oxides, the observed morphology was strongly related to the detected phases. At low temperatures, the amorphous samples (Fig. 7a) exhibited a heterogeneous grain distribution, with large particles (30–10 μm) surrounded by small ones (1–2 μm). The grains had smooth surfaces without porosity, and the very clear fracture plane t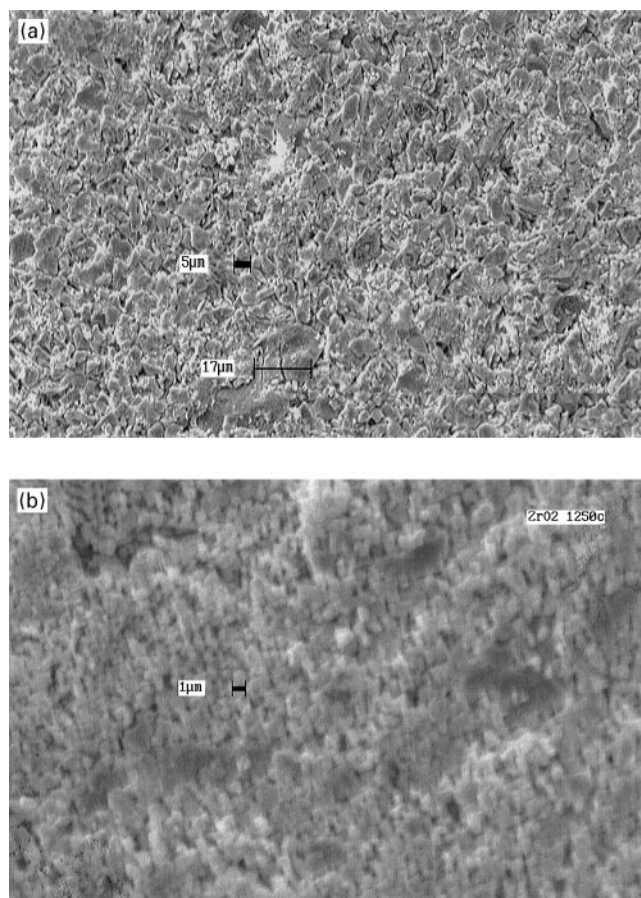ypical of glassy materials (50). Morphology changed in the crystalline samples, the grains having irregularly shaped surfaces and rough, bent fractures (Fig. 7b). Similar characteristics were observed at higher temperatures (1200–1400°C) in all compositions.

EDXA was used to obtain the qualitative Zr/Si atomic ratio and to confirm that no macroscopic phase separation took place during the synthesis or thermal treatment of the oxides. For this purpose, several measurements were carried out at different points within the samples, all of which indicated constant Zr/Si ratios.

4. CONCLUSIONS

Samples containing zirconia, silica, and mixed oxides were prepared using the sol–gel technique with alcoxides. These were consecutively annealed at temperatures from 100 to 1400°C, in increments of 100°C, 14 h per increment, with a total annealing time of 182 h. Thermal decomposition and crystallization behavior of the sample compositions was analyzed via XRD and DTA/TGA. The use of
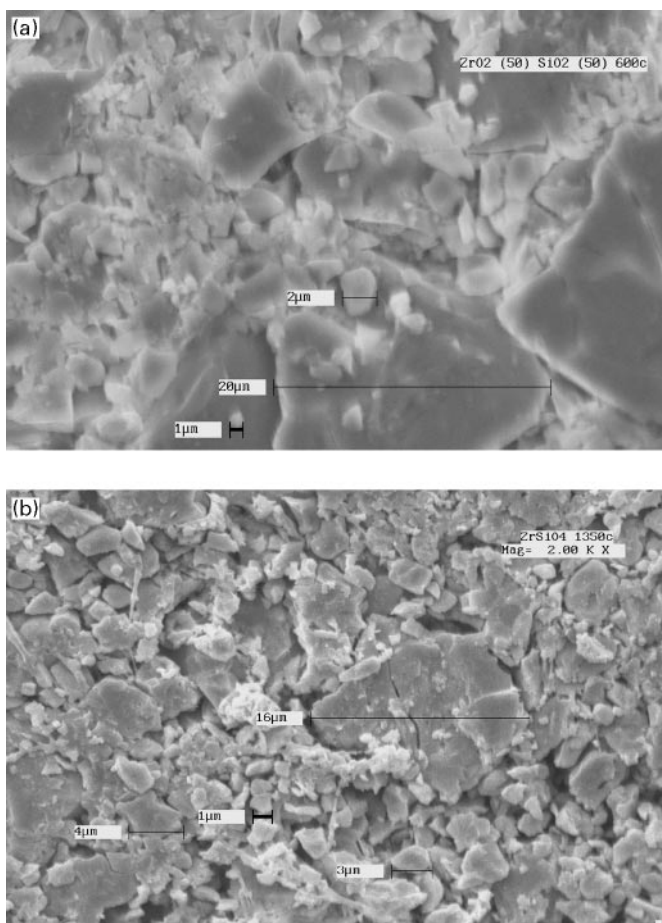
FIG. 7. SEM micrographs showing morphology change with temperature for $50ZrO_2:50SiO_2$ composition. Grain distribution at: (a) 600°C (2000×) and (b) 1350°C (2000×).

these two techniques was very effective in analyzing the crystallization stages of tetragonal zirconia, its stabilization, and transformation into the monoclinic phase in compositions with different SiO_2 amounts.

A metastable ZrO_2–SiO_2 phase diagram is presented. The coexistence region between the tetragonal zirconia and amorphous silica extended over a wide range of compositions and temperatures. At higher zirconia contents ($< 5\%$ SiO_2) Z(t) crystallization occurred at very low temperatures (approx. 300°C). Through DTA it was shown that this crystallization occurred in two stages. First, zirconia substituted silicon atoms in the ZrO_2–SiO_2 network and then, as heat increased, ZrO_2 nanoparticles segregated toward the surface and spread into the silica matrix. This allowed crystallization of Z(t) from amorphous zirconia to take place at two temperature ranges: 400–600°C and 900–1000°C.

A polymorphic tetragonal–monoclinic transformation region was observed in zirconia-rich compositions, meaning that the critical size of the tetragonal–monoclinic transformation decreased as SiO_2 content increased. Crystallite size was a critical factor determining at what temperature Z(t) transforms into Z(m).

The morphological analysis showed that by increasing zirconia content, a higher homogeneous grain distribution occurs. The loss of glassy material characteristics was obtained.

ACKNOWLEDGMENTS

REFERENCES

1. J. Brinker and G. Scherer, "Sol–Gel Science." Academic Press, San Diego, 1985.
2. L. C. Klein, *Ann. Rev. Mar. Sci.* **15,** 227 (1985)
3. A. J. Burgraaf and K. Keizer, *in* "Inorganic Membranes: Synthesis, Characteristics and Applications" (R. R. Bhave, Ed.), p. 10. Van Nordstrand-Reinhold, New York, 1991.
4. B. E. Yoldas, *J. Sol–Gel Sci. Tech.* **1,** 65 (1993).
5. T. Lopez, M. Asomoza, L. Razo, and R. Gomez, *J. Non-Cryst. Solids* **108,** 45 (1989).
6. S. J. Teichner, G. A. Nicolaon, M. A. Vicarini, and G. E. E. Gardes, *Adv. Colloid Interface Sci.* **5,** 245 (1976).
7. T. Lopez, A. Romero, and R. Gomez, *J. Non-Cryst. Solids.* **127,** 307 (1991).
8. T. Lopez and R. Gomez, *in* "Sol–Gel Optics: Processing and Applications" (L. C. Klein, Ed.), Chap. 16, p. 345. Kluwer, Boston, 1994.
9. C. Sanchez and J. Livage, *New J. Chem.* **14,** 513 (1990).
10. K. Tanabe, *Mater. Chem. Phys.* **13,** 347 (1985).
11. G. T. Mamott, P. Barnes, S. E. Tarling, S. L. Jones, and C. J. Norman, *J. Mater. Sci.* **26,** 4054 (1991).
12. D. R. Acosta, O. Novaro, T. Lopez, and R. Gomez, *J. Mater. Res.* **10,** 1397 (1995).
13. D. A. Ward and E. I. Ko, *Chem. Mater.* **5,** 956 (1993).
14. T. Lopez, J. Navarrete, R. Gomez, O. Novaro, F. Figueras, and H. Armendaris, *Appl. Catal. A* **125,** 217 (1995).
15. R. Stevens, "Zirconia and Zirconia Ceramics." Magnesium Elektron pub. No 113, 1986.
16. G. Monros, M. C. Marti, J. Carda, M. A. Tena, P. Escribano, and M. Anglada, *J. Mater. Sci.* **28,** 5852 (1993).
17. M. Vallet-Regi, S. Nicolopoulos, J. Roman, J. L. Martinez, and J. M. Gonzalez-Cabret, *J. Mater. Chem.* **7,** 1017 (1997).
18. M. Dechamps, B. Djuricic, and S. Pickering, *J. Am. Ceram. Soc.* **78,** 2873 (1995).
19. A. Gulino, R. Egdell, and I. Fragala, *J. Mater. Chem.* **6,** 1805 (1996).
20. A. Gulino, R. Egdell, G. Baratta, G. Compagnini, and I. Fragala, *J. Mater. Chem.* **7,** 1023 (1997).
21. V. S. Nagarajan and K. J. Rao, *J. Mater. Sci.* **24,** 2140 (1989).
22. F. F. Lange, *J. Mater. Sci.* **17,** 225 (1982).
23. Z. Zhan and H. C. Zeng, *J. Mater. Res.* **13,** 2174 (1998).
24. R. Gomez, T. Lopez, X. Bokhimi, E. Muñoz, J. L. Boldu, and O. Novaro, *J. Sol–Gel Sci. Tech.* **11,** 309 (1998).
25. T. Lopez, F. Tzompantzi, J. Navarrete, R. Gomez, J. L. Boldu, E. Muñoz, and O. Novaro, *J. Catal.* **181,** 285 (1999).
26. C. Morterra, G. Cerrato, and V. Bolis, *Catal. Today.* **17,** 505 (1993).

27. J. B. Miller and E. I. Ko, *Adv. Catal. Nanostruct. Mater.* **2,** 21 (1996).

28. I. M. Miranda-Salvado, C. J. Serna, and J. Ma. Fernandez-Navarro, *J. Non-Cryst. Solids.* **100,** 330 (1988).

29. I. M. Miranda-Salvado and J. Ma. Fernandez Navarro, *Bol. Soc. Esp. Ceram. Vidr.* **7,** 31-C (1992).

30. M. Andrianainarivelo, R. Corriu, D. Leclerq, H. Mutin, and A. Vioux, *J. Mater. Chem.* **6,** 1665 (1996).

31. K. Kamiya, S. Sakka, and Y. Tatemichi, *J. Mater. Sci.* **15,** 1765 (1980).

32. R. Dal Maschio, M. Filiponi, G. D. Soraru, and G. Carturan, *Am. Ceram. Soc. Bull.* **71,** 204 (1992).

33. S. W. Wang, X. X. Huang, and J. K. Guo, *J. Mater. Sci.* **32,** 197 (1997).

34. M. Nogami, *J. Non-Cryst. Solids* **69,** 415 (1985).

35. D. J. Suh and T. J. Park, *J. Chem. Mater.* **8,** 509 (1996).

36. T. Lopez, M. Asomoza, and R. Gomez, *Thermochim. Acta* **223,** 233 (1993).

37. R. P. Denkewicz, Jr., K. S. TenHuisen, and J. H. Adair, *J. Mater. Res.* **5,** 2698 (1990).

38. A. Clearfied, *J. Mater. Res.* **5,** 161 (1990).

39. X. Bokhimi, A. Morales, O. Novaro, M. Portilla, T. Lopez, F. Tzompantzi, and R. Gómez, *J. Solid State Chem.* **135,** 28 (1998).

40. A. Chatterjee, S. K. Pradhan, A. Datta, M. De, and D. Chakravorty, *J. Mater. Res.* **9,** 253 (1994).

41. P. B. Becher, *J. Am. Ceram. Soc.* **75,** 493 (1992).

42. Powder Diffraction File, International Center for Diffraction Data (ICDD), Pennsylvania, USA (1998).

43. G. Teufer, *Acta Crystallogr.* **15,** 1187 (1962).

44. C. J. Howard, R. J. Hill, and B. E. Reichert, *Acta Crystallogr. B* **44,** 116 (1988).

45. U. Martin, H. Boysen, and F. Frey, *Acta Crystallogr. B* **49,** 403 (1993).

46. M. Moran Pineda, S. Castillo, T. Lopez, R. Gomez, Cordero-Borboa, and O. Novaro, *Appl. Catal. B* **542,** 1 (1999).

47. W. Butterman and W. Foster, *Am. Mineral.* **52,** 880 (1967).

48. F. Tzompantzi, Ph.D. thesis, UAM-Iztapalapa, (2000)

49. B. D. Cullity, "Elements of X-Ray Diffraction." Addison-Wesley, Massachusets, 1978.

50. J. Ma. Fernandez-Navarro, "El Vidrio: Constitucion, Fabricacion, Propiedades." Coedited by the Consejo Superior de Investigaciones Cientificas and Instituto de Ceramica y Vidrio, Madrid, 1985.